A Brief Review on Triple Active Bridge DC-DC Converter

Subhradip Mukherjee
Department of Electrical Engineering
National Institute of Technology, Rourkela
Odisha, India
221EE4443@nitrkl.ac.in

Indrajit Sarkar
Department of Electrical Engineering
National Institute of Technology, Rourkela
Odisha, India
sarkari@nitrkl.ac.in

***Abstract*—An isolated dc-dc Triple active bridge (TAB) converter comprises three active bridges interlined using a three winding high frequency transformer (HFT). The TAB converter has advantages like controllable bidirectional power flow with high efficiency, fixed frequency operation. In the present article a brief review on TAB converter is provided for its different configurations, power flow controls and applications are analysed from research works from past few years. Controls for phase-shift and duty cycle, as well as decoupled power flow management, are also discussed. Conditions for achieving zero voltage switching (ZVS) range are also discussed.**

***Index Terms*—Isolated DC-DC Converter, Triple Active Bridge, Duty Cycle Control, Decoupled Power Flow Control**

I. Introduction

As we move towards the exhaustion of fossil fuel reserves, hybrid renewable energy sources are in high demand; they can be utilised in hybrid and fuel cell vehicles, as renewable energy generating units, and for uninterruptible power supplies (UPS). Nevertheless, the power level, voltage level, and voltage-current attributes of loads and energy storage units vary considerably. Therefore, a multiport converter interfaces these hybrid energy sources, energy reserves and loads to assimilate them under one Energy Management System (EMS). A multiport converter can integrate multiple diverse energy sources and energy storage devices, by combining their advantages. One of the key aspects of the multiport converter is the bidirectional controlled power flow capability, so that they can be used in distributing electrical power in suitable applications.

Apart from bidirectional power flow, load and high voltage ports are required to be galvanically isolated for achieving greater reliability [1]. The fully isolated TAB converters are built around an HFT, which not only provides galvanic isolation between ports but also allows for large voltage boost and eradicates leakage currents. The TAB converters are mainly designed using three active-half or full bridges. The power transfer between the different ports are governed by the corresponding phase shift angles between the ac sides of the active bridges.

The three port bidirectional converter is first mentioned in [2],where a three-port converter is designed utilising a fuel cell/battery combination to enhance the fuel cell stack's sluggish transient response. Using only fuel cell hinders the performance of the system since it has slow dynamics and lacks in energy storing capability, thus a battery pack is required and hence integrated using the three port converter to improve the system dynamics and to recover the braking energy.

In [3] the technique of General Harmonic Approximation (GHA), which is used to establish the power dynamics among the ports in the system, is employed to provide a comprehensive explanation of the TAB structure. Furthermore, the switching losses were also reduced by extending the ZVS range. To decrease net conduction losses, an optimized method with regulated parameters is devised, and the suggested approach achieves a 97.6% efficiency. Decoupling power flow and the impact of varying loads on secondary-port and tertiary-port, however, are not taken into account, thus cannot be implemented for a generalized solution.

II. TAB Converter Topologies

The general configuration of TAB converter consists of three full bridges composed of power electronic switches and a high frequency transformer (HFT). In this configuration, HFT's leakage inductances need to be accounted for since they play the key role in transferring power from one port to another. For an isolated DC-DC converter, the switching frequency must be high if the converter is to provide a high power density while being compact and lightweight.

Topology reported in [4] consists triple half bridges in Current-Current-Voltage (C-C-V) fashion, where there are a couple of current-fed ports with a single voltage-fed port. This topology is considered to be appropriate for interfacing a Battery Unit (BU) and Ultra-capacitor (UC), shown in Fig. 1(b). In this topology, each bridge consists two active switches with anti-parallel diodes and two dc filter capacitors.Using current-fed sources has the benefit of less current ripple during steady state BU and UC operation. Also the availability of current mode control provides more flexibility of the converter operation. In the proposed converter topology, optimum performance of the converter can be obtained for low and variable voltages, and high current applications. This topology is mentioned in [5] ,which is a modified version of [6], where pulse width modulation (PWM) is applied to the

979-8-3503-9874-8/23/$31.00

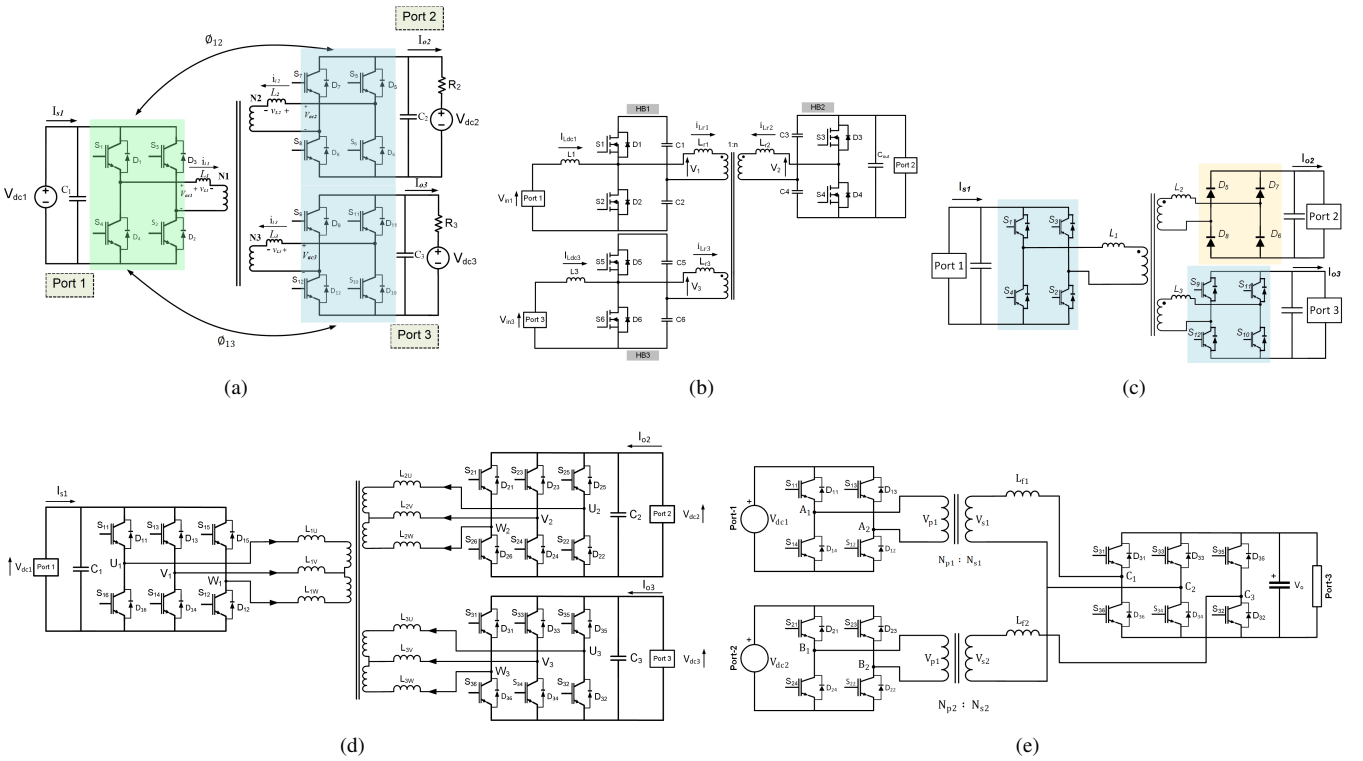

Fig. 1. TAB Converter Topologies. (a) Conventional configuration, (b) Triple Half Bridge Topology [4]–[6], (c) Diode Bridge Topology, (d) Three-phase three port topology [7], [8], (e) Dual Transformer based asymmetric TAB converter [9]

THB converter's power flow control in conjunction to phase-shift control. Multiple PI regulators regulate the duty cycle to control the power output and input voltage.

In [7], [8], the use of three-phase in TAB converter is also explored. To make the converter suitable for high power applications and higher current handling capabilities, three-phase bridges are introduced. Previous implementations of this strategy include a Dual Active Bridge (DAB) converter [10]. This design uses a three-port, three-winding symmetrical transformer to connect the three inputs and three outputs of a three-stage, six-step mode converter with regulated phase-shifts as shown in Fig. 1(d). The reduced Volt-Ampere rating of filter capacitors is a key benefit of this setup due to the use of three-phase. In addition, the system's flexibility in handling a wide range of input voltages is a significant benefit.

A new topology for TAB is proposed in [9], where two full-bridges, a three-leg converter and two HFTs are used, to isolate the source and load ports. Compared to three-winding transformer-based TAB, the proposed DT-ATAB permits operation with a wider range of phase delays, greater magnitude variation, and lower circulating currents. The three-leg converter present on the load side, consists six active switches.It is shown that the efficiency is greater than 91% throughout a wide range of output power and has a peak efficiency better than 93.7%.

A. Operation of a Conventional TAB Converter

The schematic of a conventional TAB converter is shown in Fig. 1(a). The power transfer among three ports happen, by giving appropriate gate turn on/off signals to the circuit. In the given circuit, the gate signals between port1 and port2 are delayed by ϕ_{12}, and between port 1 and port 3 are delayed by ϕ_{13}. The circuit schematic of a TAB converter is expressed using equivalent star and delta connected circuits [11], [12] as depicted in Fig. 2(a) and 2(b) respectively. In the delta equivalent circuit of the TAB, the port voltages V_{ac1}, V'_{ac2} and V'_{ac3} are primary referred square wave voltages and L_{12}, L_{13} and L_{23}, r_{12}, r_{13} and r_{23} are the equivalent leakage inductances and resistances between every two ports, respectively. In a TAB, the relative phase changes between each port determines the power transmission between them, and the power is transferred via the leakage inductance of the HFT [13]. The application of three-winding HFT introduces tightly coupled power equations that complicates the power flow control [14]. The equivalent inductances L_{12}, L_{13} and L_{23} can be calculated from transformer leakage inductances L_1, L_2 and L_3 as follows:

$$\left.\begin{aligned} L_{12} &= \frac{L_1L_2 + L_2L_3 + L_3L_1}{L_3} \\ L_{23} &= \frac{L_1L_2 + L_2L_3 + L_3L_1}{L_1} \\ L_{31} &= \frac{L_1L_2 + L_2L_3 + L_3L_1}{L_2} \end{aligned}\right\} \tag{1}$$

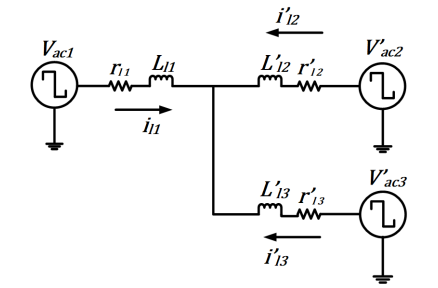

(a)

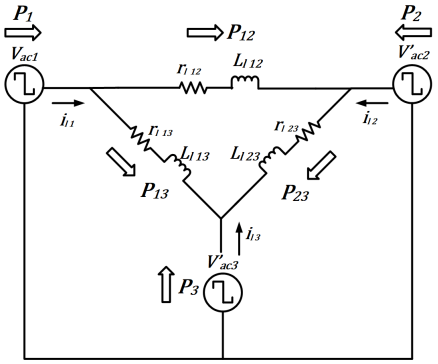

(b)

Fig. 2. Equivalent circuits of TAB converter. (a)Y connected. (b)Δ connected.

The direction of power flow from port *i* to *j* can be denoted as P_{ij}. According to [10], assuming Single Phase Shift (SPS) control and with a constant duty of 0.5, the equations for power transfer are as:

$$P_{ij} = \frac{V_i V_j}{\omega_s L_{ij}} \phi_{ij} \left(1 - \frac{\phi_{ij}}{\pi}\right) \tag{2}$$

$$\left.\begin{aligned} P_1 + P_2 + P_3 = 0 \\ P_1 = P_{12} + P_{13} \\ P_2 = P_{23} - P_{12} \\ P_3 = -P_{13} - P_{23} \end{aligned}\right\} \tag{3}$$

B. Power Flow Analysis

The phase differences between ports define the direction and magnitude of the power, which if controlled in a desired way, can be used to obtain required amount of power at the output ports [15]. As shown in 3, there are total possible six modes of power flows that can be obtained amongst the ports of a TAB converter. The same combinations has been shown in a tabular fashion in TABLE III, where, if a power P_{ij} is +ve, it denotes that power flows from port i to port j and -ve denotes that the power flows from port j to port i. The sign of phase shift governs the course of power transfer [16]. It has been analyzed from [17], that the port whose phase shift is more lagging, will have more dissipation of power in that port. For example, in case of a Lithium ion battery, present in port 3, if the battery SOC (State of Charge) is less than the rated SOC, then ϕ_{13} will have to be increased such that the power dissipated in that port will be more. Power flow in these ports occur from leading to lagging phase angles, which is also shown in Fig. 3. Using (2) and (3), all the respective port powers can be calculated.

C. Circulating and Leakage Power Flow

The difference of ac voltage magnitudes leads to propagation of circulating currents owing to the presence of leakage inductance in the HFT [18]. In the later mentioned paper, prevention of leakage power is achieved using a capacitor mounted in series with the leakage inductance. Also the power transfer between the source ports have been comparatively increased by the use of blocking capacitor.

For having zero circulating power flow the inside the system the following condition has to be ensured:

$$P_{12} + P_{23} + P_{31} = 0 \quad (4) \qquad \phi_{23} = \phi_{13} - \phi_{12} \quad (5)$$

From (3) and (4), following values of power can be obtained:

$$\left.\begin{aligned} P_{12} = -\frac{2}{3}P_2 - \frac{1}{3}P_3 \\ P_{23} = \frac{2}{3}P_2 - \frac{1}{3}P_3 \\ P_{13} = -\frac{1}{3}P_2 - \frac{2}{3}P_3 \end{aligned}\right\} \tag{6}$$

According to [4], total circulating power loss between every port is calculated as

$$P_{loss} = r_{12}(I_{12})^2 + r_{23}(I_{23})^2 + r_{13}(I_{13})^2 \tag{7}$$

where, r_{12}, r_{23} and r_{13} are equivalent resistances between every port shown in Fig. 2, I_{12}, I_{23} and I_{13} are RMS values of fundamental component of currents between three ports.

D. Phase Shift Control and Region of Operation

Altering the phase-shifts between any two bridges is another way to manage the power flow in a TAB converter. Moreover, desired phase-shift value can be chosen from a common region of operation by expanding (3) and by choosing a particular value of power. Let ϕ_{12} = x, ϕ_{13} = y, P1 = $\pm$K1, P2 = $\pm$K2, and P3 = $\pm$K3 where + denotes power being delivered and - denotes power being absorbed. To find the boundaries or region of operation for desired amount of power, following equations can be derived which can be further plotted to get the optimum phase shift angle.

$$\left.\begin{aligned} a_1x^2 - b_1y^2 - c_1\pi x + \pi y - d_1xy = \pm K_1 \\ a_2x^2 + b_2y^2 - c_2\pi x - d_2\pi y = \pm K_2 \\ a_3x^2 + b_3y^2 - c_3\pi x + \pi y - d_3xy = \pm K_3 \end{aligned}\right\} \tag{8}$$

where, a_1, a_2, a_3, b_1, b_2, b_3, c_1, c_2, c_3, d_1, d_2 and d_3 are constants. Using (8) the range of phase-shifts can be determined to obtain the desired amount of power at the output ports. Fig. 4 showcases the inductor voltage and current

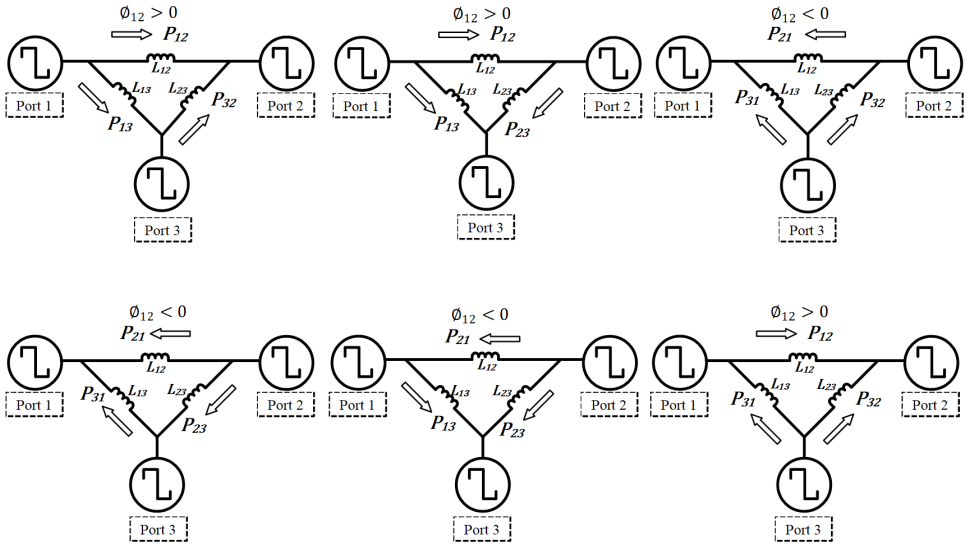

Fig. 3. Six modes of power flow in TAB for varying phase shifts

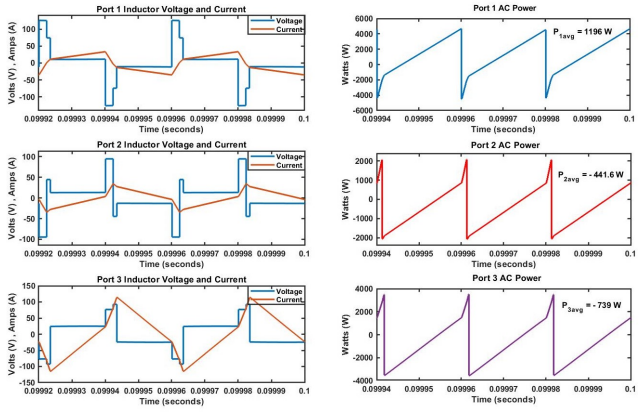

(a) (b)

Fig. 4. Waveforms of (a) Inductor Voltage and Current. (b) AC Power.

waveforms as well as the AC power waveforms at the three ports of the TAB converter for ϕ_{12} = 10° and ϕ_{13} = 15°. Fig. 4 illustrates the waveforms for inductor voltage and current along with AC power evaluated after the H-bridges of the TAB. The simulated waveforms were obtained for $\phi_{12} = 10°$ and $\phi_{13} = 15°$.

E. Duty Cycle Control

Barring the phase-shift control, variation of duty cycle is also introduced in [16], to have more degrees of freedom and to minimize the net losses. The duty cycles of the three full-bridges are defined as δ_1, δ_2 and δ_3 for the respective ports, whose control range are given from 0 to $\pi/2$. SPS control is extensively employed for TAB converters in a variety of applications, while the combination of duty cycle and phase shift control can also be implemented for light-load operations [1]. The limitation of SPS control is it leads to constrained

TABLE I
DIRECTION OF PORT POWERS WITH VARIATION IN PHASE SHIFTS

Phase Shifts			**Port Powers**		
$\phi_{13} - \phi_{12}$	ϕ_{12}	ϕ_{13}	P_{12}	P_{13}	P_{23}
<0	>0	>0	+	+	-
>0	>0	>0	+	+	+
<0	<0	<0	-	-	-
>0	<0	<0	-	-	+
>0	<0	>0	-	+	+
<0	>0	<0	+	-	-

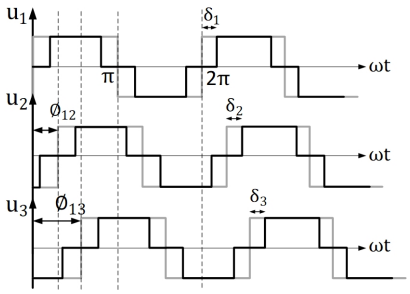

Fig. 5. Combined Duty Cycle and Phase Shift control waveforms.

ZVS operating range and significant device current stress, hence not effective for wide voltage variations [19]. Triple-phase-shift (TPS) control offers total five degrees of freedom, which minimizes the copper loss, conduction loss and also extends the range of ZVS. The conditions for Combined Duty Cycle (CDC) control and Phase Shift Control (PSC) is shown in TABLE II.:

TABLE II
DIFFERENT MODULATION TECHNIQUES AND THEIR CONDITIONS

Modulation Techniques	Conditions
SPS Control:	$\delta_1 = 0, \delta_2 = 0, \delta_3 = 0, \phi_{12} \neq 0, \phi_{13} \neq 0$
EPS Control [10]:	$\delta_1 \neq 0, \delta_2 = 0, \delta_3 = 0, \phi_{12} \neq 0, \phi_{13} \neq 0$
DPS Control [20]:	$\delta_1 = \delta_2 = \delta_3 \neq 0, \phi_{12} \neq 0, \phi_{13} \neq 0$
TPS Control [16]:	$\delta_1 \neq \delta_2 \neq \delta_3 \neq 0, \phi_{12} \neq 0, \phi_{13} \neq 0$

TABLE III
DIFFERENT CONTROL FACTORS IN DECOUPLING NETWORK

Reference Papers	x_i	x_o	y_i	y_o	z_2	z_3
[16]	$\Delta I_2'^*$	$\Delta I_2'$	$\Delta I_3'^*$	$\Delta I_3'$	$\Delta\phi_2$	$\Delta\phi_3$
[4]	W1	i_o	W2	V_{12}	ϕ_{12}	D_1
[11]	V^*_{os}	V_{os}	V^*_{ot}	V_{ot}	ϕ_s	ϕ_t
[12]	P_{1ref}	P_1	P_{3ref}	P_3	ϕ_{13}	ϕ_{23}
[17]	I_2^*	I_2	V_3^*	V_3	δ_2	δ_3

III. DECOUPLED CONTROL POWER FLOW IN TAB

From 2 and 3 it can be analyzed that each of the port powers P_1, P_2 and P_3 are a function of both the phase delays ϕ_{12} and ϕ_{13}. So to eliminate the inter-dependency between each port power, there is a need to implement the decoupled control system so that variation in power transmission in one port does not affect the other port powers. The decoupled network has been mentioned in several of the papers [4], [17]. The decoupling network can be formed with respect to the requirement of the load side, for example in one port output voltage can be controlled and other in other port current can be controlled [4] or in both the ports current can be controlled [16] or even port powers can be controlled [12]. Small signal analysis of the system is used to generate the decoupling matrix, followed by the deduction of the control-to-output transfer function. The goal of the decoupling matrix is to segregate a multivariate control system into a succession of single-loop subsystems [16], done using independent loop controllers $G_{PI2I}(s)$ and $G_{PI3I}(s)$. In Fig. 7 a block diagram of decoupling network has been shown where **G** matrix represents the small signal transfer function matrix of the converter and **H** matrix represents the transfer function matrix of the decoupling network and is found to be the inverse of the **G** matrix, as shown below:

$$\begin{bmatrix} x_o \\ y_o \end{bmatrix} = \begin{bmatrix} G_{11} & G_{12} \\ G_{21} & G_{22} \end{bmatrix} \begin{bmatrix} z_2 \\ z_3 \end{bmatrix}$$

$$\begin{bmatrix} z_2 \\ z_3 \end{bmatrix} = \begin{bmatrix} H_{11} & H_{12} \\ H_{21} & H_{22} \end{bmatrix} \begin{bmatrix} (x_i - x_o)G_{PI2I}(s) \\ (y_i - y_o)G_{PI3I}(s) \end{bmatrix}$$

where, values of x_o, y_o, x_i, y_i, z_2 and z_3 are from Table III.

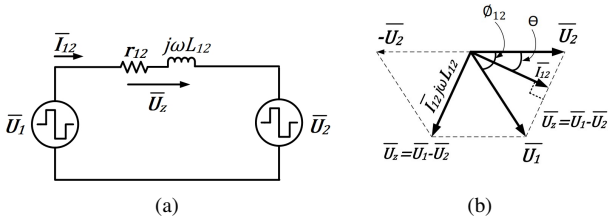

Fig. 6. TAB converter (a) circuit, (b) phasor diagram for two ports.

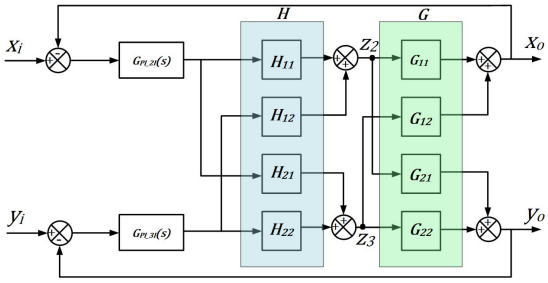

Fig. 7. Decoupling Network Matrix for Power Flow Control.

IV. ZVS ANALYSIS

The ZVS operation in isolated bidirectional dc-dc converters is proposed in [21] which was later implemented for THB in [5]. Under soft-switching conditions, high efficiency can be achieved at higher switching frequencies. Different control mechanisms are further employed to improve the range of ZVS at the trade-off of greater control complexity [22]. In order to achieve ZVS for all the devices in each of the bridges, two conditions need to be fulfilled [22]: a). The energy stored in the leakage inductance immediately before the switching transition has to be sufficient enough to charge and discharge the output parasitic capacitances of each switch, b). Dead time should be long enough to allow the resonant transition to complete before the device turns on.

V. APPLICATIONS OF TAB CONVERTER

The use of TAB in dc microgrids are discussed in [23] which shows its utilisation to cut down on the number of communication lines and dc-dc converters, thus reducing system cost. Use of TAB in dc microgrid system provides much flexibility in overall system operation. The TAB in independent dc microgrid is proposed in [24]–[26] and for household applications. In [27], TAB is proposed for UPS system and Fuel cell powered UPS is proposed in [2], [28]. For electric vehicles, TAB is used for on-board chargers of power range 3 to 6 kW. DC-DC converters combined with charger can be used in TAB as discussed in [29]–[31]. TAB can be used to regulate power flow in electric aircraft consisting of battery and fuel cell systems, and storing the energy in light load conditions to provide aid during full load conditions [32]. In [14], TAB is designed to facilitate the power transfer among the hybrid electric aircraft's generator, battery, and propulsion motor load. Conducive to increment

in the availability and dependability of the power distribution in data centres, TAB is proposed in [33], to prohibit faults in the power distribution. To reduce the number of converters, a battery can be shared among two distribution lines. Use of TAB for power management to achieve enhanced reliability and flexibility, a design is proposed in [34]. Controlling power flow improves dc grid stability and efficiency [8]. TAB for MVDC grid is proposed in [27].

Conclusion

This paper provides a brief review on the state of art and current researches done on TAB converter. Various topics regarding TAB converters that are reported so far in the literature is tried to cover. One important aspect of the TAB converter is concluded as the power flow control besides decoupled power flow control, for which several techniques are reported in the literature. Since the TAB can be operated for wide range of inputs, many ZVS analysis techniques are employed to minimize the losses as mentioned in some recent works. To provide flexibility in the range of outputs, duty cycle control along with phase-shift control is also mentioned.

References

[1] V.-L. Pham and K. Wada, "Applications of triple active bridge converter for future grid and integrated energy systems," *Energies*, vol. 13, no. 7, 2020.

[2] J. L. Duarte, M. Hendrix, and M. G. Simoes, "Three-port bidirectional converter for hybrid fuel cell systems," *IEEE Trans. Power Electron.*, vol. 22, no. 2, pp. 480–487, 2007.

[3] S. Zou, J. Lu, and A. Khaligh, "Modelling and control of a triple-active-bridge converter," *IET Power Electron.*, vol. 13, no. 5, pp. 961–969, 2020.

[4] L. Wang, Z. Wang, and H. Li, "Asymmetrical duty cycle control and decoupled power flow design of a three-port bidirectional dc-dc converter for fuel cell vehicle application," *IEEE Trans. Power Electron.*, vol. 27, no. 2, pp. 891–904, 2012.

[5] H. Tao, J. L. Duarte, and M. A. M. Hendrix, "Three-port triple-half-bridge bidirectional converter with zero-voltage switching," *IEEE Trans. on Power Electron.*, vol. 23, no. 2, pp. 782–792, 2008.

[6] H. Tao, A. Kotsopoulos, J. Duarte, and M. Hendrix, "Triple-half-bridge bidirectional converter controlled by phase shift and pwm," in *Proc. 21st Annu. IEEE Appl. Power Electron. Conf. and Expo., 2006. APEC '06.*, 2006, pp. 7 pp.–.

[7] H. Tao, J. L. Duarte, and M. A. M. Hendrix, "High-power three-port three-phase bidirectional dc-dc converter," in *2007 IEEE Ind. Appl. Annual Meeting*, 2007, pp. 2022–2029.

[8] M. Neubert, A. Gorodnichev, J. Gottschlich, and R. W. De Doncker, "Performance analysis of a triple-active bridge converter for interconnection of future dc-grids," in *Proc. IEEE Energy Conv. Cong. Expo. (ECCE)*, 2016, pp. 1–8.

[9] V. N. S. R. Jakka, A. Shukla, and G. D. Demetriades, "Dual-transformer-based asymmetrical triple-port active bridge (dt-atab) isolated dc–dc converter," *IEEE Trans. on Ind. Electron.*, vol. 64, no. 6, pp. 4549–4560, 2017.

[10] R. De Doncker, D. Divan, and M. Kheraluwala, "A three-phase soft-switched high-power-density dc/dc converter for high-power applications," *IEEE Trans. Ind. Appl.*, vol. 27, no. 1, pp. 63–73, 1991.

[11] A. Chandwani, A. Mallik, and A. M. Kannan, "A novel decoupled control scheme for phase controlled triple active bridge," in *Proc. 47th Annu. Conf. IEEE Ind. Electron. Society*, 2021, pp. 1–6.

[12] M. Phattanasak, R. Gavagsaz-Ghoachani, J.-P. Martin, B. Nahid-Mobarakeh, S. Pierfederici, and B. Davat, "Control of a hybrid energy source comprising a fuel cell and two storage devices using isolated three-port bidirectional dc–dc converters," *IEEE Trans. Ind. Appl.*, vol. 51, no. 1, pp. 491–497, 2015.

[13] N. H. Adarsh S., "Duty ratio control of three port isolated bidirectional asymmetrical triple active bridge dc-dc converter." *Int. J. Power Electron. and Drive Syst. (IJPEDS)*, vol. 12, no. 2, pp. 943–956, June 2021.

[14] C. M. Ivey, "Development of a hybrid-electric aircraft propulsion system based on silicon carbide triple active bridge multiport power converter," vol. 175, 2021.

[15] K. Nishimoto, Y. Kado, R. Kasashima, S. Nakagawa, and K. Wada, "Decoupling power flow control system in triple active bridge converter rated at 400 v, 10 kw, and 20 khz," in *Proc. IEEE 8th Int. Symp. on Power Electron. for Distr. Gen. Syst. (PEDG)*, 2017, pp. 1–6.

[16] C. Zhao, S. D. Round, and J. W. Kolar, "An isolated three-port bidirectional dc-dc converter with decoupled power flow management," *IEEE Trans. on Power Electron.*, vol. 23, no. 5, pp. 2443–2453, 2008.

[17] K. Katagiri, K. Nishimoto, S. Nakagawa, S. Okutani, Y. Kado, and K. Wada, "Decoupling power flow control of triple-active bridge converter with voltage difference between each port for distributed power supply system," in *Proc. 20th European Conf. Power Electron. and Appl. (EPE'18 ECCE Europe)*, 2018, pp. P.1–P.9.

[18] R. Rai and N. R. Tummuru, "Circulating and leakage power flow elimination technique between source ports in triple active bridge topology," in *Proc. IEEE Int. Conf. Power Electron., Smart Grid and Renewable Energy (PESGRE2020)*, 2020, pp. 1–6.

[19] J. Huang, Y. Wang, Z. Li, and W. Lei, "Unified triple-phase-shift control to minimize current stress and achieve full soft-switching of isolated bidirectional dc–dc converter," *IEEE Trans. Ind. Electron.*, vol. 63, no. 7, pp. 4169–4179, 2016.

[20] D.-D. Nguyen, G. Fujita, and M. C. Ta, "A new soft-switching strategy for three-port converter to be applied in ev application," in *Proc. IEEE 3rd Int. Future Energy Electron. Conf. and ECCE Asia (IFEEC 2017 - ECCE Asia)*, 2017, pp. 1126–1131.

[21] F. Peng, H. Li, G.-J. Su, and J. Lawler, "A new zvs bidirectional dc-dc converter for fuel cell and battery application," *IEEE Trans. on Power Electron.*, vol. 19, no. 1, pp. 54–65, 2004.

[22] L. Jiang and D. Costinett, "A triple active bridge dc-dc converter capable of achieving full-range zvs," in *Proc. IEEE Appl. Power Electron. Conf. and Expos. (APEC)*, 2016, pp. 872–879.

[23] Y. Kado, D. Shichijo, I. Deguchi, N. Iwama, R. Kasashima, and K. Wada, "Power flow control of three-way isolated dc/dc converter for y-configuration power router," in *Proc. IEEE 2nd Int. Future Energy Electron. Conf. (IFEEC)*, 2015, pp. 1–5.

[24] Y. Kado, D. Shichijo, K. Wada, and K. Iwatsuki, "Multiport power router and its impact on future smart grids," *Radio Science*, vol. 51, no. 7, pp. 1234–1246, 2016.

[25] K. Nishimoto, Y. Kado, and K. Wada, "Implementation of decoupling power flow control system in triple active bridge converter rated at 400v, 10kw, and 20khz," *IEEJ J. Ind. Appl.*, 2018.

[26] S. Nakagawa, J. Arai, R. Kasashima, K. Nishimoto, Y. Kado, and K. Wada, "Dynamic performance of triple-active bridge converter rated at 400 v, 10 kw, and 20 khz," in *Proc. IEEE 3rd Int. Future Energy Electron. Conf. and ECCE Asia (IFEEC 2017 - ECCE Asia)*, 2017, pp. 1090–1094.

[27] G. Engelmann, A. Sewergin, M. Neubert, and R. W. De Doncker, "Design challenges of sic devices for low- and medium-voltage dc-dc converters," in *Proc. Int. Power Electron. Conf. (IPEC-Niigata 2018 - ECCE Asia)*, 2018, pp. 3979–3984.

[28] H. Tao, J. L. Duarte, and M. A. M. Hendrix, "Line-interactive ups using a fuel cell as the primary source," *IEEE Trans. Ind. Electron.*, vol. 55, no. 8, pp. 3012–3021, 2008.

[29] S. Y. Kim, H.-S. Song, and K. Nam, "Idling port isolation control of three-port bidirectional converter for evs," *IEEE Trans. Power Electron.*, vol. 27, no. 5, pp. 2495–2506, 2012.

[30] Z. Ling, H. Wang, K. Yan, and J. Gan, "Optimal isolation control of three-port active converters as a combined charger for electric vehicles," *Energies*, vol. 9, no. 9, 2016.

[31] S. Y. Kim, I. Jeong, K. Nam, and H.-S. Song, "Three-port full bridge converter application as a combined charger for phevs," in *Proc. IEEE Vehicle Power Prop. Conf.*, 2009, pp. 461–465.

[32] F. Giuliani, G. Buticchi, M. Liserre, N. Delmonte, P. Cova, and N. Pignoloni, "Gan-based triple active bridge for avionic application," in *Proc. IEEE 26th Int. Symp. Ind. Electron. (ISIE)*, 2017, pp. 1856–1860.

[33] Y. Yu, K. Masumoto, K. Wada, and Y. Kado, "Power flow control of a triple active bridge dc-dc converter using gan power devices for a low-voltage dc power distribution system," in *Proc.IEEE 3rd Int. Future Energy Electron. Conf. and ECCE Asia*, 2017, pp. 772–777.

[34] Y. Yu and K. Wada, "Simulation study of power management for a highly reliable distribution system using a triple active bridge converter in a dc microgrid," *Energies*, vol. 11, no. 11, 2018.